Conference on Modelling Fluid Flow (CMFF'18)
The 17th International Conference on Fluid Flow Technologies
Budapest, Hungary, September 4-7, 2018

A STOCHASTIC APPROACH TO INVESTIGATE THE INCOMPRESSIBLE TEMPORALLY DEVELOPING TURBULENT BOUNDARY LAYER

Rakhi[1,2], Heiko SCHMIDT[2]

[1] Corresponding Author. Tel.: +49 355 69 4813, E-mail: rakhi.rakhi@b-tu.de
[2] Chair of Numerical Fluid Mechanics and Gas Dynamics, Department of Mechanical Engineering, Electrical and Energy Systems, BTU Cottbus-Senftenberg, Siemens-Halske-Ring 14, 03046 Cottbus, Germany.

ABSTRACT

In the present study, we focus on a new application of the One-Dimensional Turbulence (ODT) model to a temporally developing turbulent boundary layer. Due to dimensionality reduction in ODT, this model achieves major cost reductions as compared to full 3D simulations and is, thus, able to explore large parameter regimes, which may be very interesting for DNS. The model is fully and deterministically resolved for the diffusion effects along a 1-D domain, while the turbulent advection effects are represented by means of mapping events. Here, we apply the model for the first time to incompressible temporally developing turbulent boundary layers and compare our results to DNS [1]. We use no-slip and impermeable boundary conditions at the top and the bottom wall. We compare the velocity statistics i.e. mean, root mean square and cross stresses to the recent DNS data for Re_b = 500,1000,1500,2000. The comparison suggests that ODT is capable to reproduce several DNS velocity statistics which makes it an interesting tool to investigate higher Reynolds numbers as well as passive and active scalars in the future.

Keywords: One-Dimensional Turbulence, stochastic modeling, turbulent boundary layers, turbulent flows

NOMENCLATURE

δ_{99}	$[m]$	boundary layer thickness
Re_b	$[-]$	bulk Reynold's number
U_b	$[m/s]$	uniform velocity provided at the bottom wall
U_τ	$[m/s]$	frictional velocity
y_τ	$[m]$	viscous length scale
α	$[-]$	ODT model parameter- transfer coefficient
λ	$[s^{-1}m^{-2}]$	ODT eddy rate
ν	$[m^2/s]$	kinematic viscosity
ρ	$[kg/m^3]$	density of the fluid
τ	$[s]$	ODT eddy turnover time
θ	$[m]$	momentum thickness
C	$[-]$	ODT model parameter- Turbulence intensity
D	$[m]$	domain size
k	$[m]$	ODT kernel function
l	$[m]$	eddy size
u	$[m/s]$	velocity vector field
Z	$[-]$	ODT model parameter- viscous cut-off

1. INTRODUCTION

Numerous applications of turbulent boundary layers in the field of engineering and industry have led to rigorous study over the last decades. The simulations of turbulent boundary layers at various discrete Reynolds numbers have been carried out in [2] using a special coordinate transformation of the governing equations. Later, some studies were carried out in [3] using a temporal approach. The latter approach has been used to study compressible turbulent boundary layers in [4]. DNS of the incompressible temporally developing turbulent boundary layer is described in [1] showing that temporally and spatially developing boundary layers are similar in many respects.

In this paper, we present a lower order simulation approach, One-Dimensional Turbulence (ODT), to investigate the incompressible temporally developing turbulent boundary layer. ODT achieves major cost reduction, while covering the large Reynolds number regime as compared to the full 3D simulations. The distinctive feature of ODT, explained in [5], is that the turbulent advection is represented by a stochastic process modeling eddy motions via discrete mappings. The diffusion effects are fully and deterministically resolved along a 1-D domain. The eddy size, the time, and the location of its occurrence are chosen as a function of the local energy.

In a later study mesh adaption was implemented to further enhance the performance of the model [6]. ODT has been applied to study channel flow

[6, 7] and has also been applied to investigate complex problems like multi-physics and reacting flows [8], and to study the radiatively induced entrainment in stratiform clouds driven by cloud-top cooling [9]. Recently, ODT was used to analyse the suction boundary layers by [10]. To simulate much more complex flows and to remove restriction to one dimension, ODT is used as a subgrid model with LES referred as ODTLES [11]. These studies reveal that the model has the capability to produce results comparable with DNS in various fields. In this paper, we focus on a new application of the ODT model to study incompressible temporally developing turbulent boundary layers for the first time. The latter present a very good validation case for our model as it is statistically one-dimensional. The outline of the paper is the following. In Section 2, we discuss the formulation of the ODT model and the simulation set-up is provided in Section 3. In Section 4, we discuss the results along with a parameter study in Section 5. Our conclusions are presented in Section 6.

2. ODT

In this section the Governing Equation as well as the key ingredients of ODT are summarized.

2.1. Governing Equations

In the present study, ODT models the time evolution of a turbulent 3D flow in a 1D subspace, aligned with the wall-normal direction (y). The time evolution of the instantaneous 3D velocity vector field $\mathbf{u}(y,t)$ is described as

$$\partial_t \mathbf{u}(y,t) + EE[\mathbf{u}(y,t), y_0, l] = \nu \partial_y^2 \mathbf{u}(y,t) - \partial_x P/\rho. \tag{1}$$

In this equation, the first term represents the evolution of the velocity field with respect to time t and the second term, EE represents the advection and the pressure effects resulting from the turbulent eddy events. The first term on the right hand side represent the viscous evolution of the flow and the second term is the pressure gradient. Implementation of the eddy events of size l involves the displacement of fluid elements to represent turbulent stirring motion and modifies the velocity profile from y_0 to $y_0 + l$. This allows inter-component energy exchange. Finally, the eddies that are consistent with a turbulent kinetic energy production mechanisms in the flow are selected.

2.2. Eddy implementation

Eddy events occur through the implementation of triplet maps fulfilling the two fundamental requirements: 1) they are measure preserving, 2) they do not introduce discontinuities. The triplet map essentially takes a scalar profile in an eddy region and replaces it with three copies of the original, each compressed by a factor of three, with the middle copy inverted to avoid the discontinuities. The mapping function $f(y)$ is defined as

$$f(y) = y_0 + \begin{cases} 3(y-y_0), & y_0 \le y \le y_0 + l/3 \\ 2l - 3(y-y_0), & y_0 + l/3 \le y \le y_0 + 2l/3 \\ 3(y-y_0) - 2l, & y_0 + 2l/3 \le y \le y_0 + l \\ (y-y_0), & 0 \le y \le y_0, y_0 + l \le y \le D. \end{cases} \tag{2}$$

The mapped velocity field $\hat{\mathbf{u}}(y,t) = \mathbf{u}(f(y),t)$ is modified using a kernel function as $\hat{\mathbf{u}}(y,t) = \mathbf{u}(f(y),t) + \mathbf{c}k(y)$ to represent pressure scrambling effects, where $\mathbf{c}$ is the coefficient vector and is calculated by integrating the change of kinetic energy in a particular velocity component i due to eddy implementation over the y domain as

$$\Delta E_i = \frac{\rho}{2} \int \left[u_i(f(y),t) + c_i K(y) \right]^2 - {u_i}^2(y,t) dy. \tag{3}$$

If this expression is negative, then energy is removed from the component i and transferred to the other two components j and k as

$$\Delta E_i = -\alpha Q_i + \frac{\alpha}{2} Q_j + \frac{\alpha}{2} Q_k, \tag{4}$$

The coefficient c can be obtained by calculating the maximum extractable energy by finding the minimum of Eq. (3) and then using Eq. (3) and (4) in the equation.

2.3. Eddy selection

Mapping events are governed by an eddy rate distribution, $\lambda(y_0, l, t)$ specifying the number of eddies in the size range $[l, l + \mathrm{d}l]$, per unit length along the y-coordinate during the time interval dt. Therefore, λ should be proportional to the inverse square eddy length and an inverse time such that

$$\lambda(l, y_0, t) = \frac{C}{l^2 \tau(l, y_0, t)}. \tag{5}$$

Here, τ is related to the local flow state via energy considerations. To calculate τ, the kinetic energy of eddy turnover per unit mass $(l/\tau)^2$ is equated to the energy measure that is closely related to the maximum extractable energy of all the components, thus giving

$$\left(\frac{l}{\tau}^2\right) \sim u_{1,K}^2 + u_{2,K}^2 + u_{3,K}^2 - Z\frac{\nu^2}{l^2}. \tag{6}$$

The last term in Eq. (6) represents the viscous penalty term used as a threshold for the low-energy eddies.

2.4. ODT parameters

ODT is controlled by various model parameters discussed in [5]. The model parameter Z is used to suppress the small eddies below a certain energy threshold, e.g for $Z = 0$, eddies smaller than the Kolmogorow length scale are suppressed. This parameter increases the efficiency of the model for non bounded flows. The parameter α, controls the efficiency of inter-component energy exchange. The rate coefficient parameter, C controls the overall occurrence of the eddies and therefore the turbulent intensity. Also, the parameters L_{min}, L_p and L_{max} specify the minimum, most probable, and maximum allowed eddy size to be sampled, respectively. However, these parameters do not influence the accuracy of the output but only the efficiency of the model.

Large eddy suppression (LS) is another important feature introduced in [5] for the large eddies to avoid large-scale anomaly. The occasional occurrence of the large eddy events may dominate the total transport as their turnover time is more than the current run time of the simulations and hence these eddies should be avoided. There are different ways to restrict such large eddies explained in detail in [5].

3. SIMULATION SET-UP

The streamwise velocity component u has been initialized using a hyperbolic tangent profile as done for DNS analysis such that

$$u_0(y) = \frac{U_b}{2} + \frac{U_b}{2}\tanh\left[\frac{d}{2\Theta_{sl}}\left(1 - \frac{y}{d}\right)\right], \qquad (7)$$

where $\Theta_{sl} \sim 54\nu/U_b$ and other velocity components (v,w) are initialized to zero. All the constants used in Eq. (7) are taken from [1] to make a better comparison of the results. $d = 10^{-3}m$ is treated as constant for the present simulations. The streamwise velocity profile at $t = 0$ and at $t > 0$ is depicted in Figure 1. Dirichlet boundary conditions are used at the top and the bottom wall ($u = 0, v = 0, w = 0$) and ($u = U_b, v = 0, w = 0$) respectively.

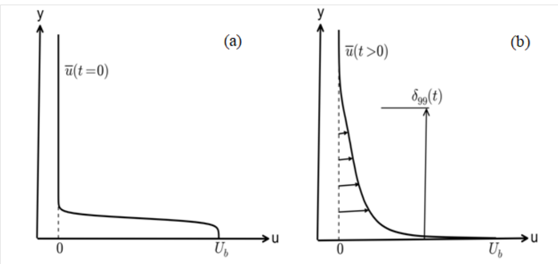

Figure 1. Velocity (in m/s) profile along the domain y (in m) at (a) t=0 and (b) t>0.

The simulations are carried out for four bulk Reynolds numbers (Re_b=500,1000,1500,2000) on a domain of $D = 43,200$, in units of ν/U_b for all cases. Re_b is proportional to the ratio of the velocity at the bottom wall and viscosity, i.e. ($Re_b = U_b d/\nu$). An explicit Euler solver with finite volume discretization is used to solve the diffusion term and turbulent advection effects are represented by means of mapping events. The code is fully parallelized running on 1000 processors. The viscosity is $1.5 \times 10^{-5}\ m^2/s$ and the pressure gradient is zero. The adaptive mesh is used to carry out the simulation and static grid to interpolate velocity values with 1500 grid points for Re_b. L_{max} is 25,920 (in units of ν/U_b), which is 60% of the domain length to avoid large scale anomaly. However, L_{min}, is different for all cases mentioned in Table 1 and $L_p = 3L_{min}$. After a detailed parametric study, the model parameters used are $C = 9, Z = 400$, $\alpha = 2/3$, and a two-thirds LS mechanism. Δy^+_{min} (smallest mesh element) and Δy^+_{max} (maximum element size) used for all the cases are summarized in Table 1 along with other parameters.

Table 1. Parameters used for the simulation with model parameter as $C = 9$, $Z = 400$, $\alpha = 2/3$, two-thirds mechanism and L_{min} and L_p are in units of ν/U_b.

Re_b	Δy^+_{min}	Δy^+_{max}	L_{min}	L_p
500	0.141	9.88	33	99
1000	0.140	9.79	10	30
1500	0.126	8.79	5	15
2000	0.065	7.91	3	9

The main control parameter in our simulations is Re_b and can be modified by changing U_b. The exact mode of transitions from laminar to turbulent is also dependent on Re_b. $u_\tau = \sqrt{\tau_0/\rho}$ where ($\tau_0 \equiv -\mu\partial\overline{u}/\partial y\ |_0 > 0$) and $y_\tau = \nu/u_\tau$ units used to scale the results into viscous '+' units.

We also define the friction Reynolds number as $Re_\tau = \delta_{99}u_\tau/\nu$, momentum Reynolds number as $Re_\theta = \theta U_b/\nu$ and displacement Reynolds number as $Re_{\delta_{99}} = \delta_{99}U_b/\nu$ for future reference.

4. RESULTS

In this section, the simulation results for different Reynolds numbers are presented. All the profiles presented are averaged across time window apart from averaging over the number of simulations. This is done to limit the effects of a single eddy on profiles of quantities and to get smooth statistics. The same domain length and grid points are used for all the simulation cases with the initial condition given in Eq. (7). A detailed parametric analysis is conducted to study their influence on the statistics presented. We have used $C = 9$, $Z = 400$, $\alpha = 2/3$ and the two-thirds LS mechanism.

Figure 2 illustrates the simulation set-up for $Re_b = 500$ at $Re_\theta = [260, 798, 1276, 1721, 2261]$ and corresponding $Re_\tau = [76, 348, 599, 829, 1083]$ from (i-v). It can be seen from the snapshots that for $Re_\theta = 260$, i.e. in the initial stage, the fluctuations are less than higher Re_θ, but with time the turbulence is propagated away from the wall and is increased for higher Re_θ. On comparing these visualizations with the different cases, it is found that the transition also depends on Re_b. It is observed that for Re_b=2000 the transition starts earlier and is further enhanced with time. However, the details of the transitions are not captured by ODT.

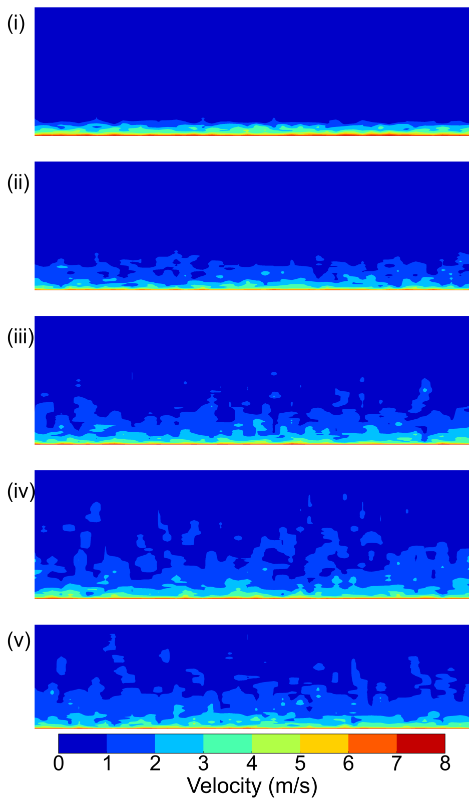

Figure 2. Velocity contours with domain on y-axis (m) and time corresponding to mentioned Re_θ on x-axis (t) for Re_b=500 at (i-v) Re_θ=[260,798,1276,1721,2261].

Figure 3 shows the streamwise mean velocity profiles and root mean square velocity profiles at $Re_\theta \sim 1968$ for Reynolds number varied in the range $Re_b = [500, 1000, 1500, 2000]$. Figure 3(a) shows the mean of the streamwise velocity as a function of the wall-normal coordinate in viscous units. The statistics are compared to DNS data reported in [1] (shown in the plot using dashed curves). The figure exhibits that, in the inner layer, i.e $y^+ < 10$, the velocity profile is independent of the Reynolds number, while in the bulk, it increases slightly with Reynolds number. Overall the profile agrees reasonably well with the DNS data.

In Figure 3(b), the root mean square of the normalized streamwise velocity component ($u^+_{rms} = \sqrt{\overline{u'^2}}/u_\tau$), as a function of normalized wall normal coordinate is shown. The peaks are under predicted compared to the DNS data. This ODT feature has already been reported in the literature, and can be avoided by retaining some 3D information of the flow [12].

Figure 4 (a) and (b) depicts the normalized cross stresses ($\overline{u'v'}/u_\tau^2$) for $Re_\theta \sim 1968$ and $Re_\theta \sim 2500$, respectively. It can be seen from Figure 4 (a) that at $Re_\theta \sim 1968$ all the curves collapse fairly well except for higher Reynolds numbers, i.e. Re_b=2000. However, when cross stresses are plotted for a later instant at $Re_\theta \sim 2500$ as shown in Figure 4 (b), a good collapse for all the Reynolds number including Re_b=2000 is observed. From this we can say that for the given initial conditions in ODT, it takes slightly longer to transition to a fully turbulent evolution than in DNS. Also, it was reported in [10] that in case of a suction boundary layer, ODT over predicts the cross stresses compared to DNS. However, in the present case for temporally developing turbulent boundary layer, the cross stresses are in very good agreement with DNS results from [1].

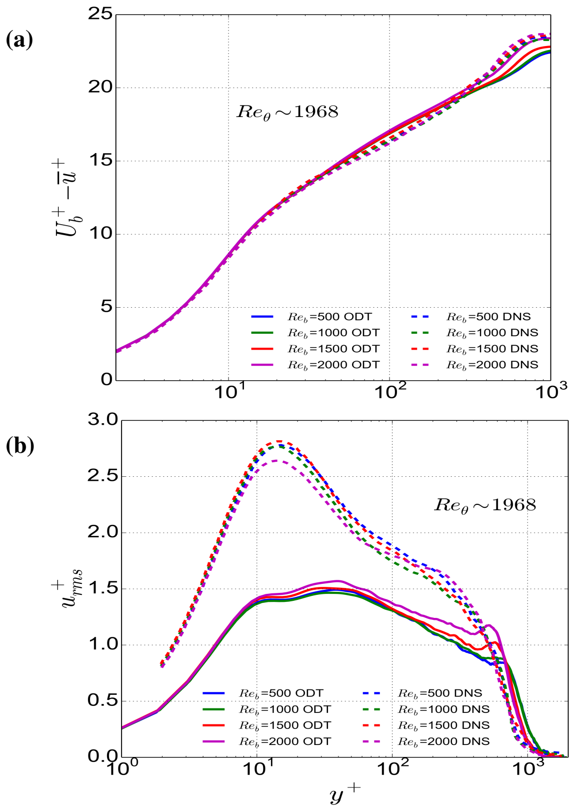

Figure 3. (a) Mean streamwise velocity profile and (b) root mean square profile, as a function of wall normal coordinate.

5. MODEL PARAMETERS

As explained earlier, ODT is governed by several parameters. Therefore, it is very important to calibrate the model parameters, in order to understand the sensitivity of the model. This also confirms the robustness of the results predicted for variation of the model parameters. We will consider the results for variations of the ODT model parameters for $Re_b = 1000$ at $Re_\theta \sim 1968$. For this paper, the results are presented for the model parameters such as the viscous cut-off parameter (Sec. 5.1), the transfer coefficient (Sec. 5.2), turbulent intensity (Sec. 5.3), and large eddy suppression (Sec. 5.4).

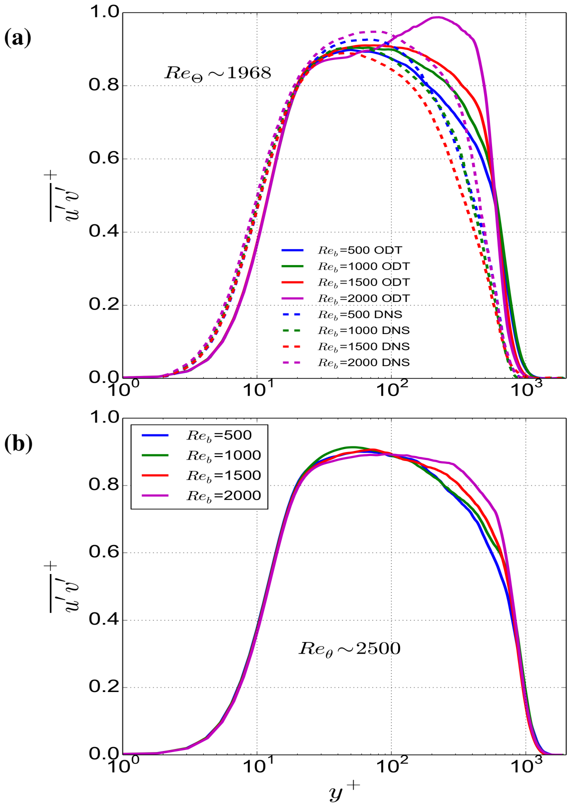

Figure 4. Cross stresses displayed as a function of wall normal coordinate at (a) Re_θ ~1968, and (b) Re_θ ~2500.

5.1. Model parameter Z

This parameter is used to suppress the small eddies to increase the performance of the model and is introduced in Eq. (6). We have varied the Z value in the range $Z = [200, 400, 600]$ while keeping other parameters constant i.e $C = 9$, $\alpha = 2/3$ and the two-thirds LS mechanism. Figure 5 depicts the influence of the parameter on (a) the streamwise velocity component, (b) rms velocity profile and (c) cross stresses as a function of wall normal coordinates.

It can be seen from Figure 5 (a) that the change of the Z parameter has no effect to the logarithmic region. Although, the change from the linear region towards the logarithmic region is highly influenced by this parameter. When $Z = 200$, then there is an earlier start of the buffer layer in the velocity profile and opposite is observed for $Z = 600$. For $Z = 400$, the profile is in good agreement with the DNS.

It is found from Figure 5 (b) that the rms of the streamwise velocity component is less sensitive to Z. Only the peaks seem to vary slightly with Z. In Figure 5 (c), cross stresses are displayed for the different Z values. It is interesting to note that, while the Z parameter showed a higher sensitivity to mean velocity profile, its impact on cross stresses was almost negligible.

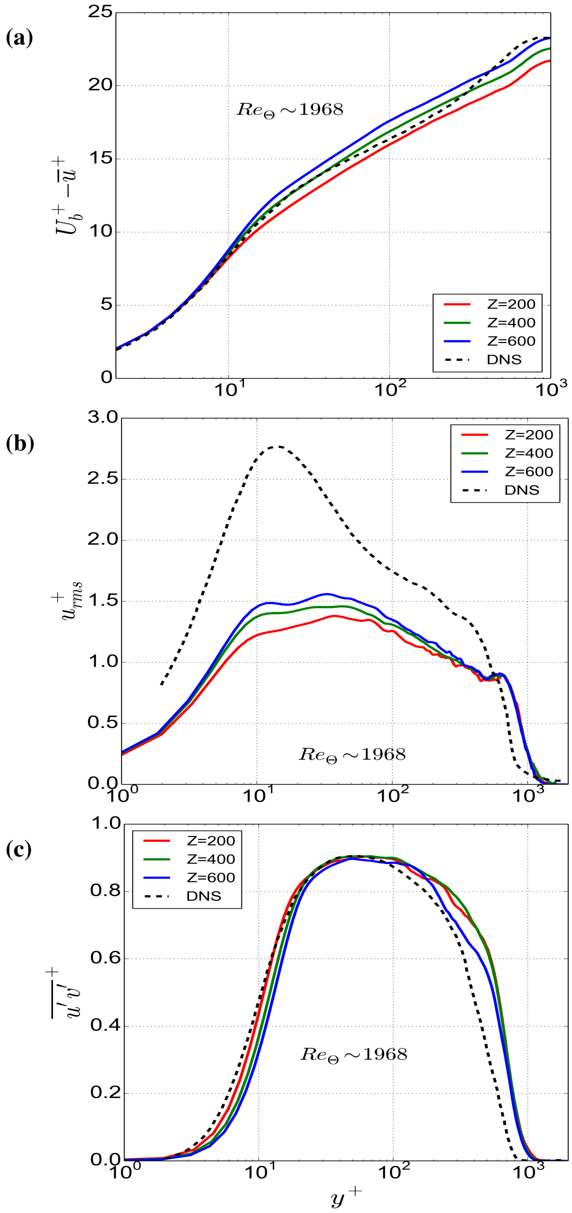

Figure 5. (a) Mean streamwise velocity profile, (b) root mean square profile and (c) cross stresses, as a function of wall normal coordinate for Re_b=1000.

5.2. Model parameter α

This parameter is introduced in Eq. (4) and controls the exchange of the turbulent energy between the three velocity components. The results for the variation of α for $Re_b = 1000$ at $Re_\theta \sim 1968$ with $C = 9$, $Z = 400$ and the two-thirds suppression method are displayed in Figure 6 for: (a) streamwise velocity component; (b) rms velocity, and (c) cross stresses, as a function of wall normal coordinate. The values for α can be in the range $\alpha\epsilon[0, 1]$, with $\alpha = 0, 2/3, 1$ corresponding to no energy exchange, equipartition of energy among the velocity components and the maximum energy exchange respectively.

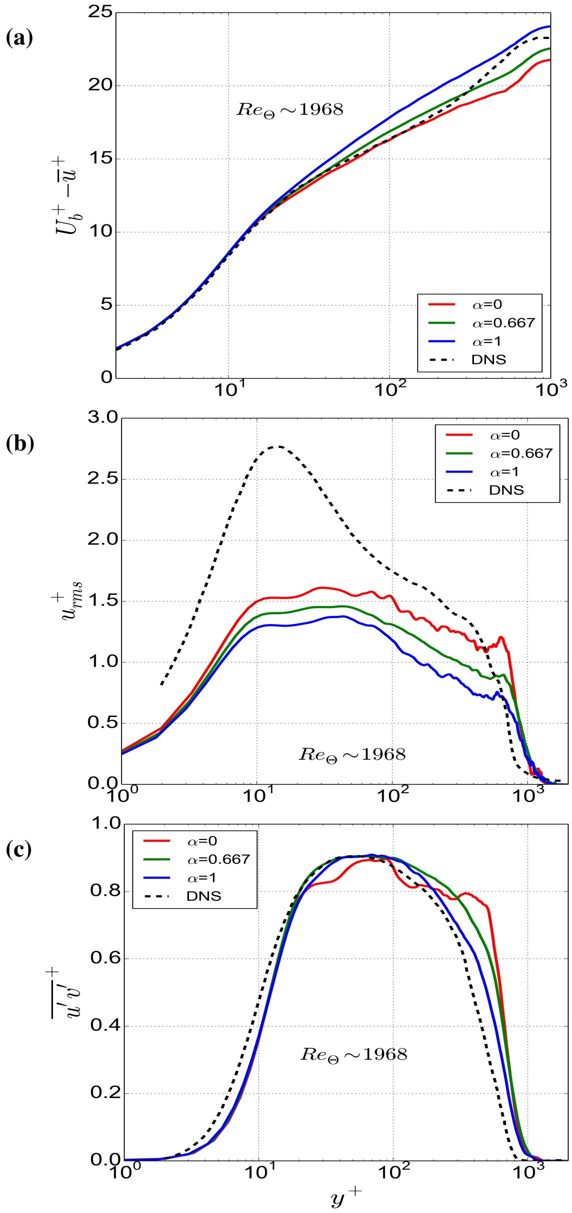

Figure 6. (a) Mean streamwise velocity profile, (b) root mean square profile and (c) cross stresses, as a function of wall normal coordinate for Re_b=1000.

Figure 6 (a) shows velocity statistics for $\alpha = 0, 1$ and $2/3$. It can be clearly seen that when there is maximum energy exchange ($\alpha = 1$), there is a shift of the buffer layer in the velocity profile and is the opposite for $\alpha = 0$. The profile matches well with the DNS results when there is equipartition of energy among the velocity components i.e. when $\alpha = 2/3$ is used.

It is found that unlike Z, α has influence on the rms velocity profile as well, although the influence is not very significant. As depicted in Figure 6 (b), the peak amplitude is maximum when there is no energy exchange and is minimum for maximum energy exchange. The amplitude increases from $\alpha = 1$ to $\alpha = 0$. Since α does not much influence the rms amplitude but has a noticeable effect on the velocity profile, $\alpha = 2/3$ was used for the present study. The influence of this parameter on cross stresses was also studied as shown in Figure 6 (c) and it was found that the cross stresses are not influenced for $\alpha = 2/3$ and 1 but in case of $\alpha = 0$, there are more fluctuations than in the other two cases.

5.3. Model parameter C

The overall occurrence of the eddies is controlled by the parameter C and is introduced in Eq. (5). The simulations are carried out for three C values i.e. $C = [6, 9, 12]$. The analysis is done for $Re_b = 1000$ at $Re_\theta \sim 1968$. While analyzing the influence of C parameter, all other parameters are kept constant as $Z = 400$, $\alpha = 2/3$ and the two-thirds suppression mechanism. Figure 7 depicts the influence of this parameter on (a) streamwise velocity, (b) rms velocity profiles and (c) cross stresses as a function of wall normal coordinates in viscous units.

It can be seen from the mean profile shown in Figure 7 (a), that the slope of the velocity profile in the logarithmic region is directly effected by C. When the rate coefficient is less i.e. $C = 6$, the velocity profile tends towards a laminar profile. In this case the level of turbulence is reduced due to implementation of less eddies. The behavior is just the opposite for large $C = 12$. The profile is closer to the DNS profile for $C = 9$.

The rms velocity is shown in Figure 7 (b). A slight change in rms values is observed with this parameter. The peak amplitude is higher for the lower value of C and less for the higher value of C. There is a slight decrease in the amplitude of rms values with increase in the value of C. As the parameter influences the velocity profile to a higher degree the value of $C = 9$ is used for the simulations. The cross stresses for this parameter, shown in Figure 7 (c), are not much influenced and are in good agreement with the DNS results for all three values of C.

5.4. Model parameter LS

To avoid large eddies, a Large Eddy Suppression (LS) mechanism is used in different ways. The simulations are performed for three different mechanisms, (i) the eddies are allowed only when the simulation elapsed time is greater than the eddy turnover time (elapsed time mechanism), (ii) when shear associated with the eddy implementation is highly concentrated in a narrow position range and causes the insertion of an eddy then this can be avoided by using the two-thirds mechanism, and (iii) simply suppress those eddies whose size exceeds a given fraction of the domain size, referred as, frac domain.

Additionally, we have presented the results when no eddy suppression mechanism is implemented (referred as none mechanism). The study is done for $Re_b = 1000$ at $Re_\theta \sim 1968$. The influence of these suppression mechanisms on (a) streamwise velocity, (b) rms velocity and (c) cross stresses as a function

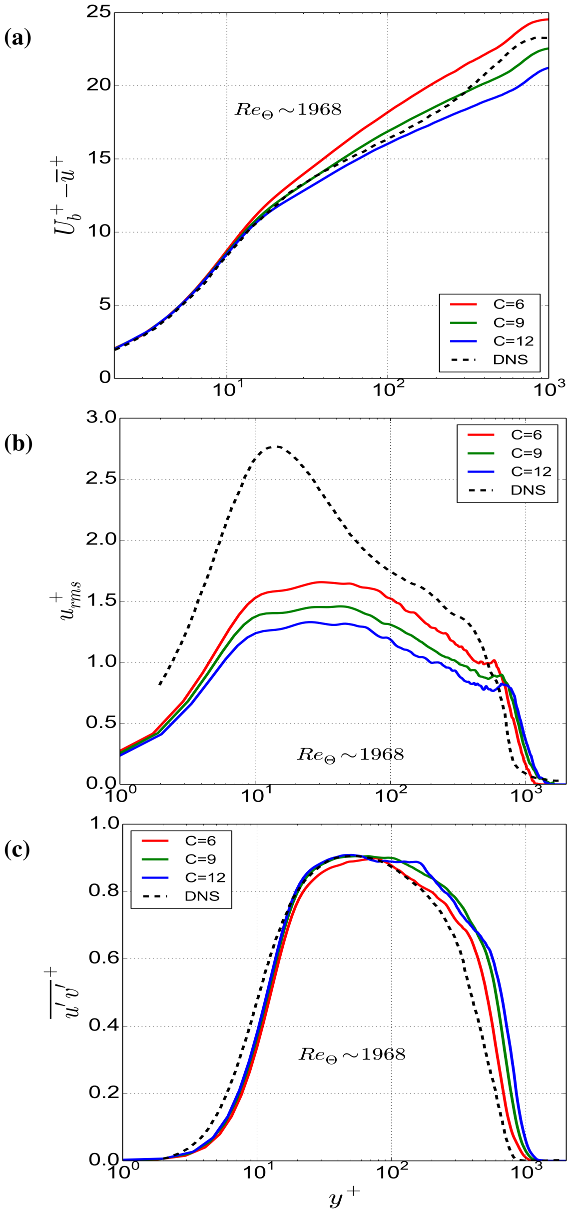

Figure 7. (a) Mean streamwise velocity profile, (b) root mean square profile and (c) cross stresses, as a function of wall normal coordinate for Re_b=1000.

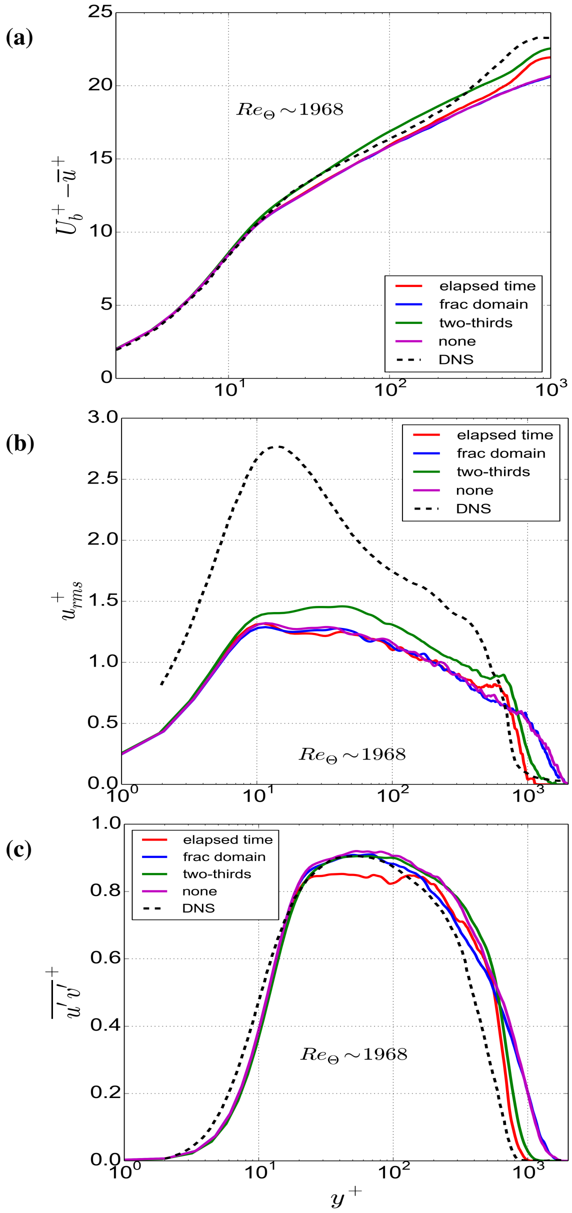

Figure 8. (a) Mean streamwise velocity profile, (b) root mean square profile, and (c) cross stresses, as a function of wall normal coordinate for Re_b=1000.

of wall normal coordinates have been presented in Figure 8. While performing the simulations with LS, all other parameters are kept constant as $C = 9$, $Z = 400$, and $\alpha = 2/3$.

In the logarithmic region, there is no influence of LS as shown in Figure 8 (a). The influence is observed in the region $y^+ > 20$ and the velocity profile agrees well with the DNS data for the two-thirds LS mechanism. On the other hand, for the other two suppression mechanisms and also when none suppression mechanism is implemented, the profile is under-predicted compared to DNS. For the elapsed time the profile in the buffer region is the same as the frac domain and none mechanism but is slightly different in outer log region. The profiles with the frac domain and none mechanism overlap with each other.

For rms profile, shown in Figure 8 (b), elapsed time, frac domain and none mechanism almost overlap with each other in the buffer region, while two-thirds show slightly more amplitude. The curves are under-predicted than DNS for all the cases. Frac domain and none mechanism vary from other two mechanisms in the outer region. Also, for cross stresses, depicted in Figure 8 (c), these two mechanisms show deviation in the outer region. For two-thirds mechanism, all velocity statistics fairly agree with DNS, so this mechanism is used for the simulations.

6. CONCLUSION

In the present study, the ODT model has been applied for the first time to simulate the incompressible temporally developing turbulent boundary layer for various bulk Reynolds numbers as $Re_b = [500, 1000, 1500, 2000]$. ODT uses a stochastic process for turbulent transport based on the energy conservation principle. The results are compared with DNS [1]. We have presented the velocity statistics i.e. mean, rms and stresses at $Re_\theta \sim 1968$, initialized with a hyperbolic tangent profile specified in Eq. (7). This investigation is further extended to analyze skin friction, shape factor, energy spectra and several evolution profiles for temporally developing turbulent boundary layer.

It is found that for model parameters $C = 9$, $Z = 400$, $\alpha = 2/3$ and the two-thirds LS mechanism, the stream-wise velocity component matches to the DNS results to a good degree. This shows the ability of ODT to capture transitions from the viscous sublayer through the buffer layer into the log layer. In case of rms velocity profiles, peak amplitude is under-predicted using ODT compared to DNS data. This behavior of ODT is already known from previous results.

Since, the ODT model is sensitive to some of its model parameters, a parametric study was conducted to analyze the influence of theses parameters on velocity statistics. The Z parameter has influence on the starting point of the buffer layer. α and C have impact on the slope of the velocity in the log region and the LS method have higher influence on the profile in the outer log region.

The rms velocity profile is influenced slightly and cross stresses are not influenced much by Z, α and C parameters. However, frac domain and none suppression mechanism have more influence on the outer region. We find that ODT agrees well with the DNS for $C = 9$, $Z = 400$, $\alpha = 2/3$ and two-thirds mechanism. All these results show that ODT has the capability to reproduce several velocity statistics for incompressible temporally developing turbulent boundary layers.

ACKNOWLEDGEMENTS

The authors thank the Graduate Research School (GRS) of the BTU Cottbus-Senftenberg for the financial support.

REFERENCES

[1] Kozul, M., Chung, D., and Monty, J. P., 2016, "Direct numerical simulation of the incompressible temporally developing turbulent boundary layer", *Journal of Fluid Mechanics*, Vol. 796, pp. 437–472.

[2] Spalart, P. R., 1988, "Direct simulation of a turbulent boundary layer up to $Re_\theta = 1410$", *Journal of Fluid Mechanics*, Vol. 187, pp. 61–98.

[3] Brereton, G. J., and Reynolds, W. C., 1991, "Dynamic response of boundary-layer turbulent to oscillatory shear", *Physics of Fluid*, Vol. A 3, pp. 178–187.

[4] Martin, M. P., 2007, "Direct numerical simulation of hypersonic turbulent boundary layers. Part 1. Initialization and comparison with experiments", *Journal of Fluid Mechanics*, Vol. 570, pp. 347–364.

[5] Kerstein, A., 1999, "One-dimensional turbulence: model formation and application to homogeneous turbulence, shear flows, and buoyant stratified flows", *Journal of Fluid Mechanics*, Vol. 392, pp. 277–334.

[6] Lignell, D., Kerstein, A., Sun, G., and Monson, E., 2013, "Mesh adaption for efficient multiscale implementation of One-Dimensional Turbulence", *Theoretical and Computational Fluid Dynamics*, Vol. 27, pp. 273–295.

[7] Schulz, F., Glawe, C., Schmidt, H., and Kerstein, A., 2013, "Toward modeling of CO_2 multi-phase flow patterns using a stochastic multi-scale approach", *Environment Earth Science*, Vol. 70, pp. 3739–3748.

[8] Jozefik, Z., Kerstein, A., Schmidt, H., Lyra, S., Kolla, H., and Chen, J., 2015, "One-dimensional turbulence modeling of a turbulent counterflow flame with comparison to DNS", *Combustion and Flame*, Vol. 162, pp. 2999–3015.

[9] Schmidt, H., Kerstein, A., Nédélec, R., Wunsch, S., and Sayler, B. J., 2013, "Analysis and numerical simulation of a laboratory analog of radiatively induced cloud-top entrainment", *Theoretical and Computational Fluid Dynamics*, Vol. 27, pp. 377–395.

[10] Fragner, M. M., and Schmidt, H., 2017, "Investigating Asymptotic Suction Boundary Layers using a One-Dimensional Stochastic Turbulence Model", *Journal of Turbulence*, Vol. 18, pp. 899–928.

[11] Schmidt, R., Kerstein, A., and McDermott, R., 2010, "ODTLES: A multi-scale model for 3D turbulent flow based on one-dimensional turbulence modeling", *Computer methods in applied mechanics and engineering*, Vol. 199, pp. 865–880.

[12] Schmidt, R., Kerstein, A. R., Wunsch, S., and Nilsen, V., 2003, "Near-wall LES closure based on one-dimensional turbulence modeling", *Journal of Computational Physics*, Vol. 186, pp. 317–355.